AIAA-2021-2610

Aerodynamic Flow Control of an Unstable Slender Cylindrical Body at High Incidence

Edward Lee [1], You Huang [2], Bojan Vukasinovic[3], and Ari Glezer[4]
Woodruff School of Mechanical Engineering,
Georgia Institute of Technology, Atlanta, GA 30332-0405

Abstract

Aerodynamic instabilities of a slender cylinder with an ogive forebody inclined at high incidence (45° < α < 60°) in a uniform stream is investigated in wind tunnel experiments. At these inclination angles the rollup of the counter-rotating forebody vortex pair becomes asymmetric and their subsequent interactions with the wire-mounted cylinder and its wake induce a nominally-stable side force whose sense depends on and varies with the azimuthal orientation of the forebody. The present investigations have shown that at some orientation of the forebody the tip vortices develop strong azimuthal oscillations that are manifested in bimodal migration in the near wake. Furthermore, the coupling to the model leads to time-varying side forces and unstable oscillations. Azimuthal actuation effected by an embedded synthetic jet at the juncture of the forebody is used to stabilize the vortex pair and thereby suppress the model oscillations. The unstable oscillations can be suppressed during pitch up/down maneuvers either ahead or following the onset of the instability.

I. Background

Investigations of the aerodynamic characteristics of axisymmetric slender bodies at moderate and high incidence angles have been largely motivated by the flight dynamics of missiles, munitions, and fighter aircraft. These flight platforms encounter complex, unsteady aerodynamic loads that are usually far more significant at higher angles of attack and are associated with the appearance and evolution of trains of spatially and temporally varying vortical structures over the body and in its near wake. The earlier studies showed that these vortical structures are spearheaded by the formation and asymmetries of counter-rotating vortex pairs successively formed beginning at the upstream end of the forebody. The dynamics and asymmetries of these forebody vortices and their interactions with vorticity concentrations within the oblique shear layers that bound each side of the near wake along the main cylindrical body and its aft segment can contribute to strong unsteady side- and cross-stream forces and yawing and pitching moments that may be used for attitude control.

[1] Graduate Research Assistant, AIAA Member.
[2] Graduate Research Assistant, AIAA Member.
[3] Research Engineer, AIAA Member.
[4] Professor, AIAA Fellow.

In one of the early investigations of the forebody vortices, Nelson and Fleeman (1975) attributed the induced changes in side force and yawing moment on the cylinder to asymmetric shedding of vortices from its leeward side. Yanta and Wardlaw (1977) noted the asymmetry of the forebody vortices and flow at high inclination angles can be caused by minor variations of the nominally axisymmetric forebody, and in a subsequent investigation (Yanta and Wardlaw, 1981) attributed the side force that occurs when one of the forebody vortices detaches from the body to the opposite sense vortex that remains attached. Subsequently, these authors found that the asymmetric vortex pattern ($\alpha = 45°$) is formed as a result of secondary vortices that develop adjacent to the primary forebody vortices, causing one of the primary vortices to become detached from the surface (Yanta and Wardlaw 1982).

Based on simulations and flow visualization studies of the forebody vortex flow over a range of angles of inclination in various studies (e.g., Wu et al., 1986, Ward and Katz 1989, Zilliac et al. 1991, and Deng et al. 2003), the topology of the forebody vortices over a range of inclination angles can be divided into three primary regimes. These regimes include: symmetric vortices that are mostly jointly located adjacent to the surface of the cylinder or become jointly detached from the surface ($\alpha < 30^o$), asymmetric vortices where one of the counter-rotating vortices become detached first, leading to mutual roll ($30° < \alpha < 60^o$) and to significant side force and yawing moment, and unsteady wake-like flow when the vortices couple to the oblique and Kármán shedding off the cylinder section ($60° < \alpha < 90^o$).

At high angles of attack, simulations of asymmetric vortex shedding induced by a geometric perturbation on one side of the forebody of a slender ogive-cylinder ($\alpha = 70°$) by Ma and Liu (2014) showed that the wake of the main cylinder can be roughly divided into two main streamwise domains. This is consistent with the observations of Thomson and Morrison (1971), where the upstream (5-7*D* long) domain comprises of a quasi-steady multi-vortex structure of the forebody vortex system, and the downstream domain is characterized by Karman vortex shedding. Ma and Liu (2014) reported a dominant wake frequency associated with each of the forebody and Kármán vortex shedding domains and noted that as the incidence increases, the upstream domain diminishes, as it can be expected. It is noteworthy that the simulations of Ma and Liu (2014) reveal interactions of the forebody vortices with streamwise vortices that form within the oblique shear layers on each side of the cylinder's near wake.

In an effort to mitigate asymmetric vortex formation and the associated increase in side forces and yawing moments, the utility of movable and/or deployable mechanical protrusions for reduction in aerodynamic side forces and moments has been investigated. Rao et al. (1987) tested deployable strakes on an isolated forebody ($L/D \approx 5$; $\alpha = 50°$) and reported large changes in the side forces with the strakes azimuthal angle that were associated with the formation of a 'strake vortex' that remained close to the forebody, or a larger scale detached 'spoiler vortex'. Leu et al. (2005) utilized an array of inflatable micro-balloon actuators fixed to the surface of a conical forebody ($L/D = 5$) to induce the formation of asymmetric vortices and side forces of a desired direction. Stucke (2006) manipulated the forces, pitch and yaw moments, and roll angle of an inclined axisymmetric body ($L/D = 4$, $\alpha = 50°$) using spoilers and strakes near the leading edge. More recently, Mahadevan et al. (2018) triggered and managed the asymmetry of forebody vortices using boundary layer scale hemispherical protrusions on a highly polished conical forebody.

A number of investigations employed fluidic actuation (steady and unsteady blowing and suction) and limited plasma actuation near the tip of inclined forebodies to manipulate the shedding of the vortices from the leeward surface and thereby effect changes in the side forces and yawing moments. Steady jets have been used over a range of subsonic and transonic speeds and momentum coefficients (e.g. Almosnino and Rom, 1981, conical forebody, $L/D = 6$, $\alpha = 35° - 55°$, $C_\mu < 0.002$, and Skow et al., 1982, ogive forebody, $L/D = 3.5$, $\alpha = 35° - 55°$). Unsteady actuation using a linear array of synthetic jets along the leeward stagnation line of a conical forebody was used by Williams et al. (1989) and Williams and Papazian (1991) to form 'pneumatic' splitter plate and effect flow symmetry at $\alpha = 55°$. Similarly, Kalyankar et al. (2018) used unsteady sweeping jets on the side of an inclined cylinder ($L/D = 9$, $\alpha = 60°$) to alter the separation line on the surface and generate yaw moment as large as $\Delta C_{LN} \sim 0.8$ with $C_\mu = 2.7\%$. The "phantom yaw" effects associated with asymmetric vortex shedding over a pitching axisymmetric body ($L/D = 20$) were characterized in the recent simulations of Schnepf and Schülein (2018), who used steady blowing from a slot along the side of the body to mimic an 'aerostrake' and to mitigate asymmetric vortex shedding and reduce the aerodynamic side force by 25%. In a noteworthy approach, Sato et al. (2016) were able to reduce the side force and yawing moment on a cone-body ($L/D = 5.7$, $\alpha < 90°$) by up to 50% by using autonomous bleed driven through internal passages within a forebody cone by the external pressure differences. Plasma actuation was used by Fagley et al. (2012) to manipulate the asymmetric aerodynamic side force on an inclined forebody (Kármán ogive, $L/D = 3.5$, $40° < \alpha < 60°$) by up to $\Delta C_Y = \pm 1$. Considering the effectiveness of active actuation, a number of investigations have demonstrated closed-loop feedback control of the aerodynamic side forces induced by the forebody vortices. For example, the methodology of Porter et al. (2014) was recently adopted by Seidel et al. (2018) in a simulated closed loop feedback controller which could effect specified side forces.

The present investigation builds on initial work by Lee et al. (2021) who exploited aerodynamic flow control approaches for prescribed modification of the wake structure and thereby the resulting side forces on a slender axisymmetric body at high incidence, up to 60°. As noted in this prior work, the unsteady coupling between the wake and the body can trigger the body instability, which was shown to be either attenuated or amplified by the applied flow control. Although such body instabilities may not be directly detectable on sting-mounted models, the model wire-support of the present experiments allows for body unsteady response to the dynamically changing wake and different aspects of its natural unstable coupling, as well as its controlled states are the primarily focus on the current investigation.

II. Experimental Setup and Procedures

The present experimental investigation utilizes the same slender axisymmetric cylinder model ($L/D = 11$, $D = 40$ mm, $Re_D = 7.9 \cdot 10^4$) that was designed and built by Lee et al. (2021), having the tangent ogive forebody of the length $l/D = 2$. The investigations are focused on control of autonomously formed forebody vortices over a range of high angles of inclination ($45° < \alpha < 60°$), while the wind tunnel was operated with uniform wind speed of $U_o = 30$ m/s, both for the model prescribed pitch α and for the pitch-up and pitch-down maneuvers.

The axisymmetric model is wire-supported in an open-return wind tunnel (test section measuring 91 cm on the side) by a dynamic 6-DOF eight-wire traversing mechanism (Figure 1) described in detail by Lambert et al. (2016). Each support wire has an in-line load cell and is controlled by an independent servo motor. The forces and moments on the model are calculated from the measured wire tensions projected onto the model (the resultant aerodynamic loads on the model are calculated relative to the loads in the absence of cross flow, and accounting for wire drag). The attitude of the model is commanded by a *Matlab Simulink* controller, which feedback utilizes

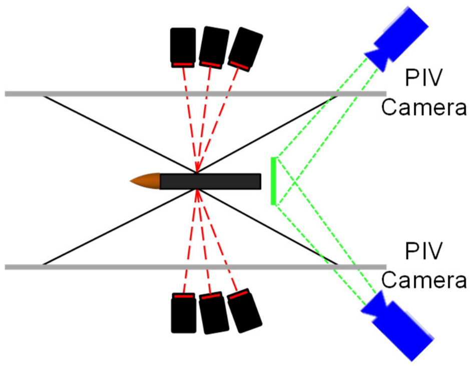

Figure 1. Schematics of the top view of the supported model illustrating the stereo PIV wake measurements and positioning of the Vicon cameras for orientation tracking of the model.

inputs from *VICON* motion-capture camera system at an update rate of 500 Hz. Besides providing the feedback signal, the six-camera motion capture system resolves the spatial and temporal position of the model at any instant in time. In an alternate configuration, the feedback loop can be disconnected and the model 'locked' in the desired attitude. Either configuration is utilized, depending on the body maneuvering. The information regarding the model position/orientation is used to extract the wire orientation and accurately decompose the forces measured on each load cell into x, y, and z components in real time. In addition to the measurement of the aerodynamic loads, a stereo PIV (SPIV) system is used to characterize the model's wake dynamics using two CCD cameras that are each placed at an angle of 20° relative to an image plane normal to the oncoming flow at x/D = 2 – 9 from the tip of the model. Schematics in Figure 1 illustrates orientations of the two PIV and six motion-capture cameras that are distributed evenly on both sides of the test section.

The axisymmetric body is comprised of three major modules: the ogive forebody, synthetic jet actuator module, and the central cylindrical body, as illustrated in Figure 2. Both the forebody and the jet module are designed such that can be rotated by the full azimuthal period. The azimuthal orientation of the forebody ϕ and the jet θ are referenced to the top vertical point, with the angles increasing clockwise, in the upstream view. The jet module incorporates a single azimuthal orifice measuring 0.6 × 15.7 mm, imparting the jet momentum coefficient C_μ while issuing normal to the surface at the frequency of about 2.3 kHz. Although the lab-fixed coordinate system is utilized for most of the presented results, including the drag, lift, and yaw forces/coefficients, unsteady motion of the model is primarily in its own yaw coordinate β', which is often used as a descriptor instead of the lab-fixed yaw β (Figure 2). In contrast to many of the prior investigations of fluidic control for affecting the symmetry of the forebody vortices, and in line with the prior work by Lee et al. (2021), in the present investigations the upstream actuation jet is deliberately placed well downstream of the forebody tip, just downstream from the termination of the forebody, as illustrated in Figure 2. For that control purpose, a single synthetic jet actuator (orifice measuring 0.6 × 15.7 mm) is integrated at the juncture between the forebody and the cylinder. The jet's azimuthal orientation θ is adjustable independently of the forebody azimuthal orientation ϕ.

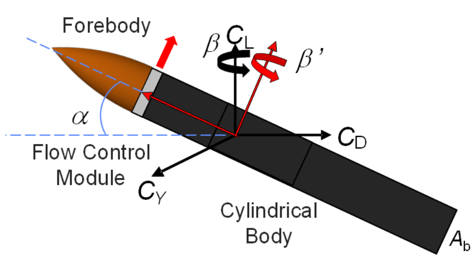

Figure 2. Axisymmetric slender model (L/D = 11) with an ogive forebody (l/D =2) having an integrated flow control module.

III. Unstable Coupling of the Forebody Vortices in the Base Flow

As shown in a number of the earlier investigations (e.g., Lamont and Kennaugh 1989, Mahadeven et al. 2018, Lee et al. 2021), induced side force switches its sign with rotation of the forebody, which is attributed to the surface imperfections. To further test this assessment, four identical forebodies (l/D = 2) are manufactured in separate processes and tested at $\alpha = 60°$ ($Re_D = 7.9 \cdot 10^4$) over a full azimuthal rotation of the forebody. The resulting drag, lift, and side force coefficients (each normalized by the cylinder's cross-sectional area A_b) are shown in Figure 3a. In concert with the earlier investigations, the side force exhibits azimuthally periodic switching for each of the forebodies, while the drag and lift coefficients remain steady and nearly identical. As the source of asymmetry is randomly associated with the azimuthal reference point ($\phi = 0°$), side force variations among the different forebodies are not in phase, such that an initial phase shift is conducted before plotting all of the results in Figure 3a. In principle, it is shown that $C_S > 0$ for most of the azimuthal orientations $100° < \phi < 220°$, $275° < \phi < 50°$ and switches direction $C_S < 0$ only within narrow azimuthal domain centered about $\phi = 70°$ and $220°$.

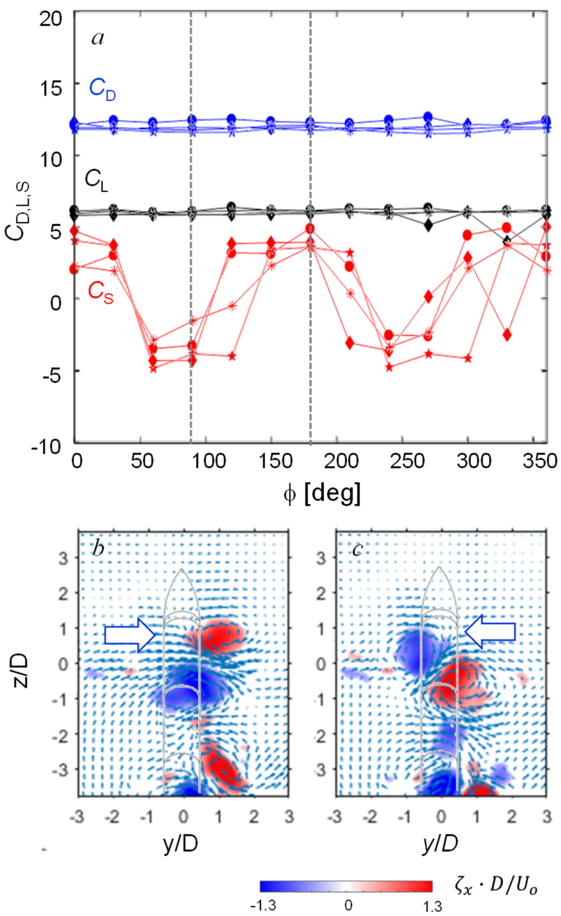

***Figure 3.** Baseline aerodynamic forces variation with the forebody azimuthal orientation ϕ for three forebodies (a), and the ensemble-averaged vorticity and velocity fields at x/D = 5 for $\phi = 90°$ (b) and $180°$ (c).*

To illustrate what changes in the wake structure are associated with the opposing-sign side forces, the two instances marked by the dashed lines in Figure 3a ($\phi = 90°$ and $180°$) are characterized by the sPIV measurements at $x/D = 5$. The resulting flow fields are shown in Figures 3b and c along with overlaid silhouettes of the projected body. As can be seen, the leading pair of the forebody streamwise vortices become detached from the surface unevenly and evolve into the asymmetric and tilted pairs, where the CCW vortex leads at $\phi = 90°$ (Figure 3b), while the CW vortex leads at $\phi = 180°$ (Figure 3c), having the tilt angle/slope of the vortex pair positive and negative, respectively. This switched imbalance/asymmetry of the leading vortex pair is responsible for the switched sign of the side force, which direction is schematically shown by the overlaid arrows in Figures 3b and c.

As noted by Lee et al. (2021), at certain prescribed forebody orientations at high incidence angles, the body can couple to its wake in an unstable fashion, where its oscillations are primarily in its own yaw direction β' (cf. Figure 2). To illustrate the difference between the body stable (but not steady) and unstable response, two characteristic realizations are shown in Figure 4, where the yaw response over time and its corresponding ensemble-averaged wake flow ($x/D = 5$) are shown for the stable (Figures 4a and b) and unstable (Figures 4c and d) coupling. As noted above, even in the absence of the strong body deflections (Figure 4a), body responds to the changing aerodynamic loads and it is never steady. Still, such deflections are of a very small amplitude. The averaged streamwise vortex pair for the stable body coupling (Figure 4b) has a strong CCW and CW vorticity signatures, indicating that these vortices are also fairly stable with time. When the body couples to its wake in an unstable fashion, strong yaw oscillations, typically in excess of ten degrees in amplitude, are observed, as seen in Figure 4c. The corresponding ensemble-averaged flow field in Figure 4d suggests that the dominant vortices are highly unstable with time, as only a weak remnant of the vortex pair is measured in the average. These aspects of the body-vortex coupling will be further addressed later in the paper.

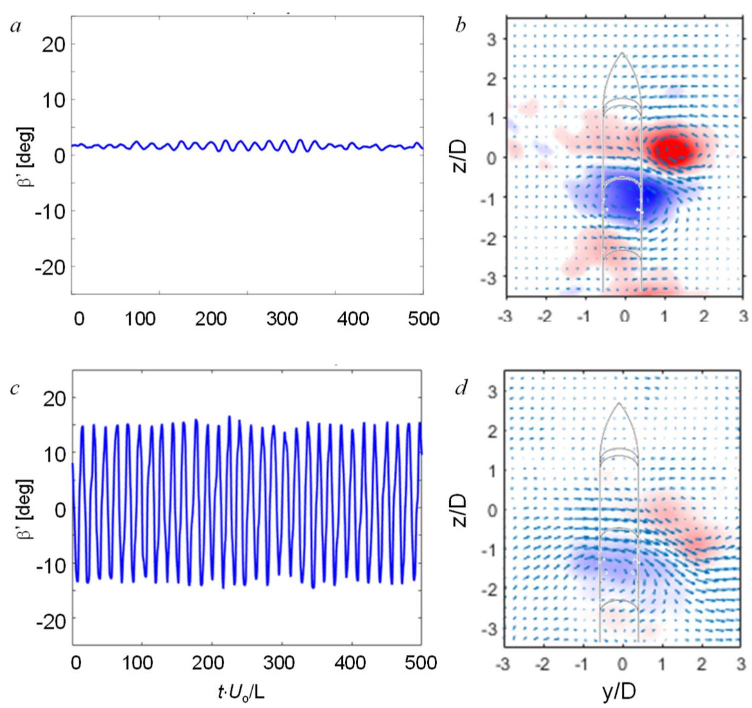

Figure 4. *The model motion in yaw β' (a,c) and the ensemble-averaged vorticity and velocity fields (b,d) for the stable (ϕ = 90°,a,b) and unstable (ϕ = 315° , c,d) body coupling. Contour levels or vorticity are the same as in Fig. 3.*

For the remainder of the paper, only one of the four forebodies analyzed in Figure 3a is utilized, and the force changes with its azimuthal orientation are shown in Figure 5a. As the primary interest of the current study is in the unstable body coupling, the forebody orientations, centered about ϕ = 270° and 330°, for which the body undergoes unstable motions are marked in gray. As an example, the realized yaw deflections β' at ϕ = 270° are shown in Figure 5b, along with its power spectra in Figure 5d. Clearly, the dominant body oscillation frequency is shown to be about 6 Hz in this instance, with the first two higher harmonics present as well. Interestingly, there is another much weaker frequency component close to 100 Hz (and its higher harmonics), which is attributed to the vortex shedding frequency off the body. Although the dominant body response during the unsteady coupling is in its own yaw direction, its prescribed pitch orientation becomes also displaced, along with the yaw oscillations. This is illustrated in Figure 5c where a phase plot of the fixed-reference pitch (body referenced pitch is by default zero) is plotted relative to its yaw deflection β'. It is interesting to note that the body actually responds to the aerodynamic loads by Lissajous oscillations in pitch and yaw, where the corresponding frequency ratio is 1:2 and the phase delay is about π/2.

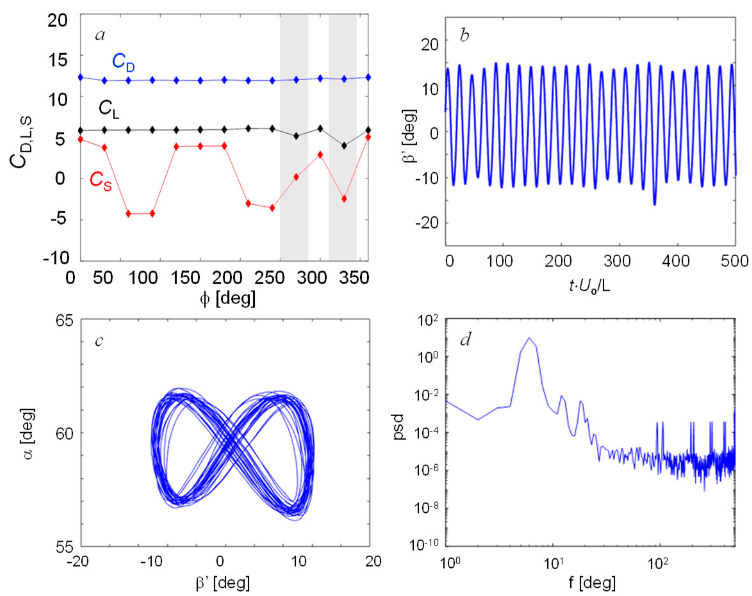

Figure 5. *Force coefficients with forebody orientation θ at a = 60° (a) and the body yaw time trace (b), phase plot of the pitch vs. yaw angle (c), and power spectra of β' (d) for the body unstable coupling for ϕ=270°.*

Aside from considering axisymmetric body at any given incidence angle that results in the body instability, another relevant scenario is examined in which the body undergoes pitch-up or down maneuvers. During these maneuvers, the model is commanded to steadily pitch up from α = 45° to 60° followed by pitch down back to 45°. The pitch

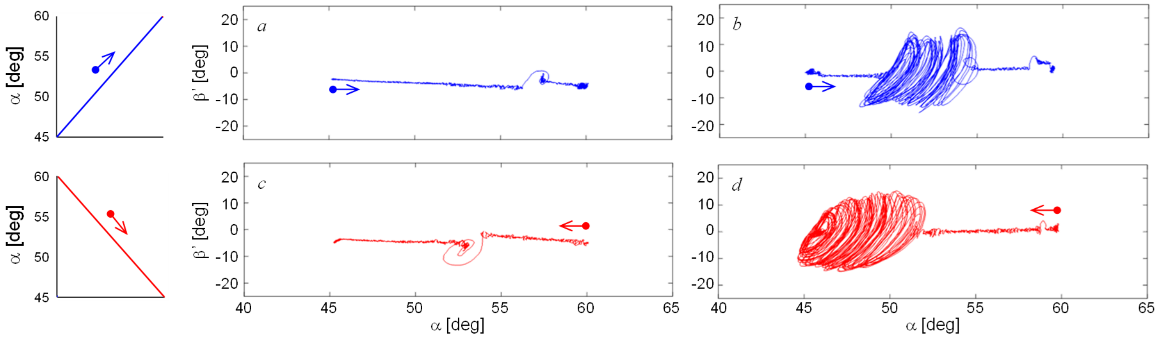

Figure 6. *Model yaw angle β' variation during the increasing (a,b) and decreasing (c,d) pitch sweep 45 ° < α < 60 ° for the forebody azimuthal orientation ϕ = 0 ° (a,c) and 30 ° (b,d).*

rates are varied over an order of magnitude, ranging from 0.1 to 1 degree/sec, and the time-varying aerodynamic loads on the model and its pitch, yaw, and roll angles are monitored to detect the onset and termination of its instability. Although some minor details of the evolution of the instability change somewhat with pitch rate, there are two scenarios that are common to all of the pitch rates and are in Figure 6. First, depending on the azimuthal orientation of the forebody ϕ, the model may be stable despite abrupt changes or disturbances in yaw in during pitch up (55º <ϕ < 60º) and down (50º <ϕ < 55º), as shown in Figures 6a and c, or unstable during pitch up (48º <ϕ < 55º) and down (45º <ϕ < 53º), as shown in Figures 6b and d. The second notable aspect of these unstable changes in trajectory is the presence of a clear hysteresis in the onset and termination of these instabilities depending on the direction of the pitch which is attributed to the different flow states when the pitch motion begins. During pitching up from α = 45°, the body wake is still dominated by the forebody vortices, whose detachment from the surface migrates closer to the forebody with increasing pitch angle and ultimately the wake becomes dominated by the cylinder itself. During pitch down, the starting wake at α = 60° is in a complex state of interactions between the cylinder shear layers and the pairs of forebody vortices and it is argued that their complex interactions suppress the appearance of the instability through a lower pitch angle. Aside from the hysteresis in onset, there does not appear to be a notable difference in terms of the amplitude of oscillations during the instability in both the pitch up and down the yaw oscillations amplitude is about ten degrees.

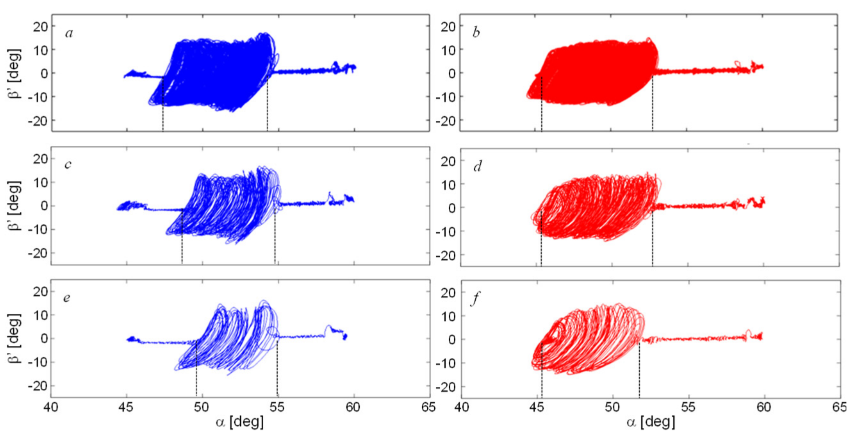

Figure 7. *Yaw angle variation during the increasing (a,c,e) and decreasing (b,d,f) pitch sweep 45 ° < α < 60 ° for the forebody azimuthal orientation ϕ = 30 ° and the pitch rate $\dot{\alpha}$ = 0.1 (a,b), 0.25 (c,d), and 1(e,f) deg/s.*

Although the two general types of responses to the pitch maneuver do not, in principle, depend on the pitch rate (0.1 – 1 deg/s), there are some differences regarding the characteristics of the pitch-induced instabilities. The dependence of the instability during pitch-up and -down motions on the pitch rate is determined by changing the pitch rate among 0.1, 0.25, and 1 deg/sec between 45° < α < 60°, and the resulting excursions in yaw β' are shown in Figure 7. As the model pitches up

(Figures 7a, c, and e), there is a consistent, albeit small, delay in the onset of the instability that the increases with pitch rate. The instability onset occurs at $\alpha \approx 50°$ at $\dot{\alpha} = 1$ degrees/sec and the overall delay from $\dot{\alpha} = 0.1$ (Figure 7a) to 1 degrees/sec (Figure 7e) is about 2°. The termination of the instability is less sensitive to the pitch rate and varies by about 1° ostensibly as a result of the transition to the wake-dominated flow around the model at high angles of incidence and is also the reason for the minor differences during pitch-down (Figures 7b, d, and f). In fact, when pitch-down commences with wake-dominated flow at high incidence, the transition to the forebody dominated flow is delayed towards lower pitch angles and extends down to $\alpha \approx 45°$ significantly lower than the onset of instability during the pitch-up motion.

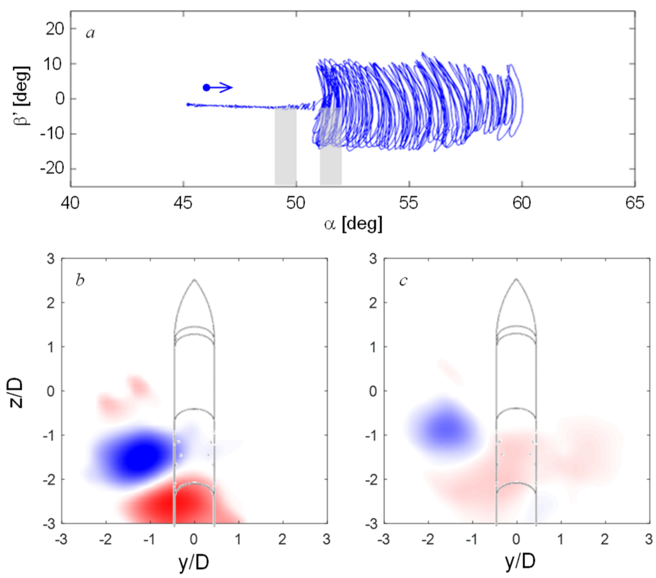

Figure 8. *Model yaw trace (ϕ = 315˚) as it pitches up from α = 45° - 60 ° (a) and ensemble-averaged vorticity field at x/D = 9 during the body stable (α = 49˚-50˚) (b), and unstable (α = 51˚-52˚) (c) coupling. Contour levels or vorticity are the same as in Fig. 3.*

As the body sets into unstable response to the changing aerodynamic loads during the pitch-up motion, it is illustrative to assess what change is observed in the topology and dynamics of the dominant forebody vortex pair. For that purpose, instability of the body pitching up at the rate of 1 deg/s (forebody orientation ϕ = 315°) is characterized in term of the yaw response β' (Figure 8a) and the two characteristic segments are selected for the wake measurements at x/D = 9 and highlighted in gray in Figure 8a. The first segment spans the pitch fraction α = 49° – 50° for which the model is stable, and the second one, α = 51° – 52°, immediately after the body commences unstable motions. The measured vortical topology for these two segments is shown in Figures 8b and c, respectively, also having a silhouette of the model projection overlaid on the plots. Similar to the wakes for the fixed incidence angle, as discussed in Figure 4, stable model response during the pitch-up motion is associated with the stable dominant forebody vortex pair, as indicated by the strong concentrations of the CW and CCW vorticity in Figure 8b. Contrary to this scenario, once the body undergoes unstable motions, significantly weakened signatures of the primary vortex pair in the averaged flow field indicate that the vortices are also dynamically changing their spatial position, while, on the average, the CW vortex still mostly leads the pair, signaling that even in the unstable motions, the prevailing side force magnitude would be positive, albeit time dependent.

Further analysis of the body and vortex pair time-dependent coupling is based on the motion tracking of the forebody tip and each of the vortex cores, extracted from the sPIV measurements (x/D = 9), where the tip location is shown in black, and CW and CCW vortex cores by the blue and red dots in Figures 9a and c, respectively, for the two segments discussed in Figure 8, when the body's coupling is stable and unstable. Additionally, each vortex pair is connected with the green line when its slope is negative and with the magenta line when positive. In addition, a subset of the yaw β' and the vortex orientation angle δ evolution over time is shown in Figures 9b and d, during the stable and unstable body coupling, respectively. The model stable response in reflected

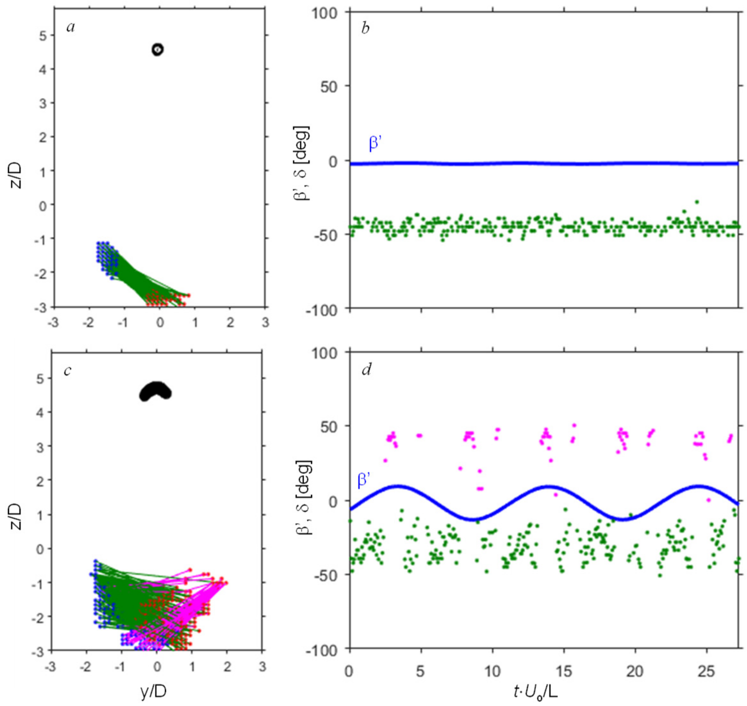

Figure 9. *The forebody tip (●) and the CW (●) and CCW (●) vortex centroid positions at x/D = 9 during the model pitch up motion during the stable (a, α = 49° – 50°) and unstable (c, α = 51° – 52°) body coupling. The corresponding positive (magenta) and negative (green) angular orientation of the vortex pair is shown for the stable (b) and unstable (d) coupling.*

by the nearly invariant forebody tip realizations over time, as seen in Figure 9a. Furthermore, it is seen in the same plot that both CW and CCW vortex realizations remain tightly clustered, having the same tilt at all times. This state is further quantified in Figure 9b, where nearly invariant β' is measured over this subset in time. At the same time, the vortex pair slope also remains nearly invariant at about δ = -45°. During the model unstable motions, it is seen that the forebody tip deflect in both pitch and yaw (as already pointed to in Figure 5c). At the same time, there is much wider scatter of the vortex cores, where the vortex pairs orientation is not preserved but rather switches in bimodal fashion, alternating between the positive and negative slopes. This is further quantified in Figure 9d. It should be noted that some vortex detections, especially during the unstable motion, do not reliably result in the detections of both vortices and such are discarded; hence there are some dropouts in the time evolutions of the vortex pair slopes in Figure 9d. Nonetheless, it can be seen in these time evolutions, relative to the model yaw, that the switching of the vortex pair orientation (i.e., the δ sign) occurs about extrema of the model yaw deflections, where the vortex pair temporarily switches its orientation on the approach to the peak excursion and then subsequently reverts back.

IV. Suppression of the Forebody Vortex Pair Instability

While the prior work on stabilization of axisymmetric bodies in 1-D (Lambert et al., 2019) and 3-D (Lambert et al., 2016) naturally unstable motions utilized the tail-end flow control due to the nominally zero angle of incidence, the present flow control focuses on the dominant forebody vortices and therefore considers the indirect upstream flow control approach discussed previously by Lee et al. (2021).

Prior of addressing the unstable body response to its wake, it is informative to assess what the flow control approach that was originally developed for the side force management (Lee et al, 2021) can effect during the pitch maneuvers that do not trigger unstable response, as already presented in Figure 6. It is shown that even in the case when the model is stable, the actuation alters the flow field during the pitch-up and -down motions. An example is shown in Figure 10, where both the model excursion

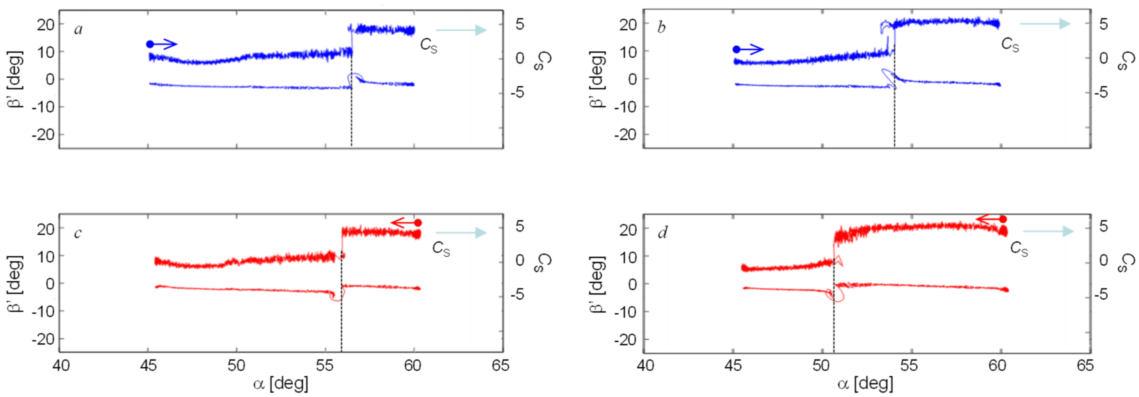

Figure 10. *Model yaw angle β' and force coefficient C_s change for the base (a,c) and controlled (b,d) flow during the pitch up (a,b) and down (c,d) α sweeps. Azimuthal orientations of the forebody and the control jet are (ϕ,θ)= (340°, 90°).*

in yaw (β') and the induced side force coefficient C_s are shown during the prescribed motion in pitch. In the absence of actuation, (Figures 10a and c during pitch-up and -down, respectively), a net positive side force during pitch-up motion (Figure 13a) indicates that the vortex asymmetry is already established at the onset of motion. The magnitude of this side force is relatively steady up until a sudden perturbation occurs as α passes 56°. The force magnitude more than doubles and it might be associated with one of the vortices being advected further into the wake, and the vortex that remains close to the surface lead to $C_S \approx 5$. Another interesting point is that this sudden change in force (and in the balance between the vortices) yields a force impulse on the model from which it recovers. A small hysteresis in the force and body yaw is evident during the pitch-down motion of the base flow (Figure 10c), when the detached forebody vortex encounters the vortex close to the surface which is marked by a sudden drop in force. The resulting moment also provides a sudden jolt in yaw from which body recovers as in the case of the pitch-up motion. As the body pitches up with the activated synthetic jet actuation (at $\theta = 90°$), the sudden force switch becomes triggered at about $\alpha = 54°$ and $C_S > 5$ for the remainder of the motion but the model recovers to nominally-steady yaw. The difference between the pitch motions in the presence and absence of actuation is even more pronounced during pitch-down. The side force increases down to about $\alpha = 51°$ (Figure 10d) compared to about $\alpha = 56°$ in the absence of actuation (Figure 10c). As shown, the actuation effectively expands the range of pitch angles for which $C_s \approx 5$ in either pitch- up or -down maneuvers.

Arguably the more interesting scenario arises when the body does couple to its wake in an unstable fashion. In that case, the unsteady response shown in Figures 6b and d, for the pitch up and down motion, respectively, is selected for the uncontrolled/natural response and plotted in Figures 11a and c. Discussion of the main features of the natural body response and of the instability hysteresis is presented in conjunction with Figure 6. Here, an open-loop flow control approach is applied while the body undergoes the same pitch maneuver, i.e., the flow control is applied while the model was still in the stable pitching motion. The resulting controlled model yaw deflections are shown in Figures 11b and d, during the pitch up and down motions, respectively. It is seen that the flow control completely bypasses the unstable states in either pitch direction, having only the small transients in yaw about the highest pitch angles.

Beyond the open-loop control, another approach is tested, where the flow control is not started before the onset of the body instability. This scenario is depicted in Figure 12a through the

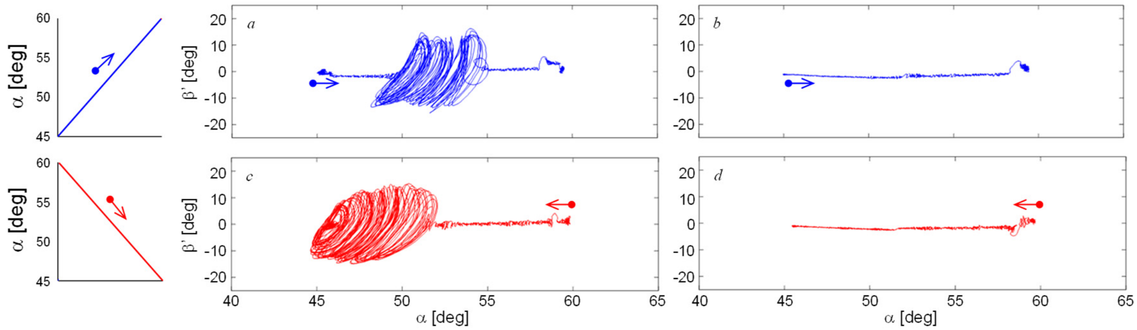

Figure 11. *Model yaw angle β' variation during the increasing (a,b) and decreasing (c,d) pitch sweep 45° < α < 60° for the forebody azimuthal orientation ϕ = 30° for naturally unstable(a,c) and the open-loop controlled (b,d) cases.*

measured model yaw deflection β' as it pitches up from $\alpha = 45°$ to 60°. Just as the model begins to undergo unstable oscillations, the flow control is activated at the point marked by the green arrow. Subsequently, over the next half a degree in pitch, the yaw oscillations become suppressed and remain stable for the duration of the flow control activation. Once the flow control is deactivated, marked by the red arrow, the model quickly diverts into high amplitude oscillations. Just as in the case of the instability onset (Figure 8), changes in the corresponding wake topology are assessed by the sPIV measurements at $x/D = 9$. Ensemble-averaged streamwise vorticity is shown in Figure 12b during the base flow pitch segment from $\alpha = 51$-52°, as the body is unstable. Similar to the unstable case shown in Figure 8c, there is a rather weak vortex signature in the mean due to the vortex unstable motions associated with the body instability. Still, the vortex structure in the mean suggests that there is a bias of the leading CW vortex in the wake, implying that there is a bias in the positive net side force during this unsteady motion. Knowing that the forebody vortices naturally coupled to the stable body response are stable themselves (e.g., Figure 9a), it is expected that the flow control stabilized body response would also couple to the stable dominant vortices. Indeed, Figure 12c indicates that the forebody vortex pair is significantly more stable compared to its counterpart in Figure 12b, as the vortex concentrations are far stronger defined in the averaged sense.

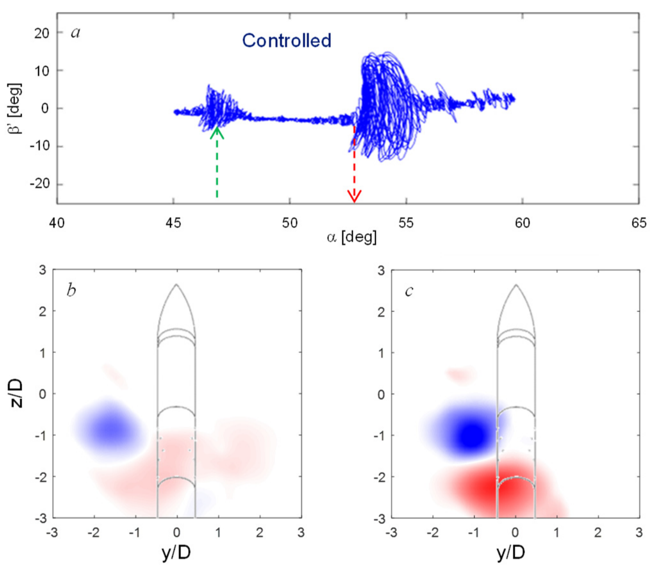

Figure 12. *Model yaw trace (ϕ=35°) as it pitches up from α = 45° - 60° (a), with the flow control activated and deactivated at the green and red arrow timing, respectively. One-second averaged vorticity field at x/D = 9 is shown for the uncontrolled (b) and controlled (c) pitch span α = 51-52°. Contour levels or vorticity are the same as in Fig. 3.*

Another extension of the flow control of an already unstable body is applied when the model undergoes fully developed unstable yaw deflections at a pre-set incidence. For that purpose, the model is positioned at $\alpha = 53°$ with the forebody orientation of $\phi = 315°$, allowing natural oscillations to develop. These oscillations are shown in blue in Figure 13a. After a number of oscillation cycles, the flow control is activated at $t{\cdot}U_o/L = 314$ and the oscillations dampened over the following about 8~10 oscillation cycles, with the body remaining stable thereafter. As long as the flow control was kept active, the

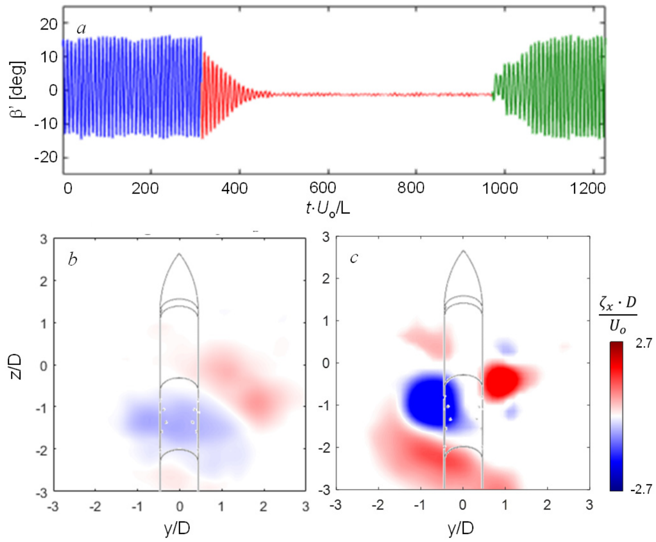

Figure 13. *Yaw trace of the model (θ =90°, ϕ= 315°) at α = 53°, where the controlled section is shown in red (a), and one-second averaged vorticity field at x/D = 9 for the uncontrolled (b) and controlled (c) flow.*

body remained stable, up to the point of its termination at $t{\cdot}U_o/L = 973$. Once the flow control is terminated, the body gradually resumes its oscillations, over longer than the 4~5 oscillation periods. The yaw trace is shown in red during the controlled segment, and once the control is terminated, the remaining trace is shown in green. Based on the previously discussed differences in the wake topology associated with the unstable and stable body response, it is expected that the flow fields associated with the naturally unstable (Figure 13b) and stabilized body (Figure 13c) would be in line with the topologies discussed for their counterparts during the pitch maneuvers (Figure 12). The vortex signatures associated with the unstable model (Figure 13b) indicate the dynamic vortex coupling to the model. In this instance, opposite to the pitch flow control (Figure 12), predominant bias in the vortex pair orientation suggests the negative side force in the average. As the body is stabilized (Figure 13c), two strong vortex signatures indicate their relative stability in the wake, too, where the CW vortex appears to induce a strong counter-rotating motion in the wake at the very bottom of the measured domain.

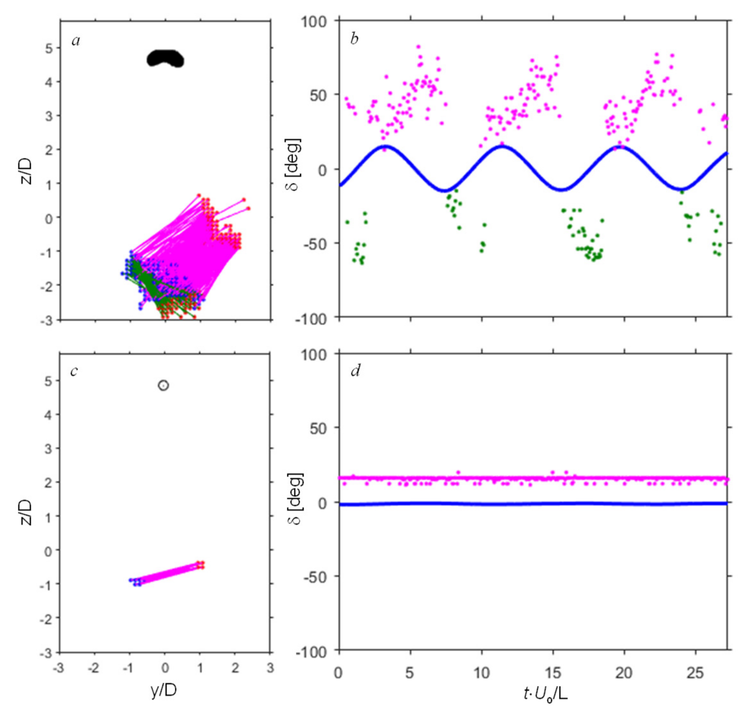

Figure 14. *The forebody tip (●) and the CW (●) and CCW (●) vortex centroid positions at x/D = 9 for the baseline (a) and controlled (b) flow α = 53°. The corresponding positive (magenta) and negative (green) angular orientation of the vortex pair is shown for the base (b) and controlled (d) flow.*

Similar to the analysis of the switch between the stable and unstable body state during the pitch up motion (Figure 9), analysis of the body and vortex pair time-dependent coupling for the uncontrolled and controlled cases shown in Figure 13 is shown in Figure 14. The data are based on the motion tracking of the forebody tip and each of the vortex cores, extracted from the sPIV measurements (x/D = 9), shown in black, blue, and red dots, and the color-coded orientations of the vortex pairs in Figures 14a and c, just as in Figures 9a and c. The accompanying plots in Figures 14b and d show a subset of the yaw β' and the vortex orientation angle δ evolution over time for the uncontrolled (Figure 14b) and controlled (Figure 14d) case. During the unstable body coupling, forebody tip's trajectory indicates predominantly yaw deflections accompanied with some pitch variations, while the vortex pair orientation switches between the two states, although its orientation is biased towards the positive tilt (Figure 14a). The difference relative to the pitch-up unstable mode (Figure 9b) is in the preferred switch of the vortex pair tilt, which occurs only on one excursion side in the model yaw, as indicated in Figure 14b. As the body becomes stabilized by the flow control, both the forebody tip (Figure 14c) and the vortex pair tilt become stabilized, having the yaw of about $\beta' = 0°$ and the tilt angle of $\delta = 20°$.

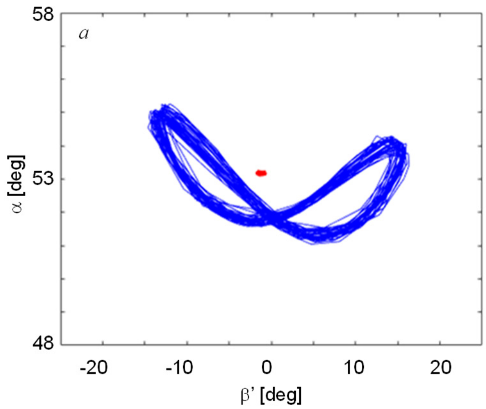

Figure 15. *Pitch and yaw variations of the baseline (blue) and controlled (red) flow, having the prescribed pitch $\alpha = 53°$.*

As seen in the tip trajectory in Figure 14a, the body responds in both the yaw and pitch deflections, in spite of being preset to $\alpha = 53°$. The body polar response is shown in Figure 15 as its pitch deflection with the yaw deflection for both the uncontrolled and controlled state discussed in Figures 13 and 14. Just as in the baseline body instability discussed in Figure 5c, the model naturally undergoes Lissajous trajectory in pitch and yaw (shown in blue), where the corresponding frequency ratio is still 1:2 but the phase delay appears to be closer to $3\pi/4$. Remarkably, the controlled pitch-yaw polar, shown in red, indicates that the flow control anchors the model to about zero degrees in yaw and the prescribed pitch of 53°.

Lastly, spectral analysis of the uncontrolled and controlled body-wake coupling is done for both the baseline unstable (Figures 16a and c) and stable (Figures 16b and d) body response. The unstable body deflection in yaw in excess of ten degrees in amplitude is measured in the uncontrolled flow, while the controlled flow stabilizes body about zero degrees in yaw (Figure 16a). The corresponding power spectra (Figure 16c) indicates the dominant natural oscillation frequency of about 8 Hz, having also the prominent its harmonic. Although the distribution of the spectral energy does not significantly change for the controlled flow, there is a slight shift towards lower dominant frequency, which for the controlled flow becomes closer to 6 Hz. Besides this change, the two spectra appear similar across frequencies and the only difference is in the drop across more than two decades in magnitude. As noted earlier (Figure 4), even though the most body responses do not exhibit strong deflections and are not deemed 'unstable', the body always

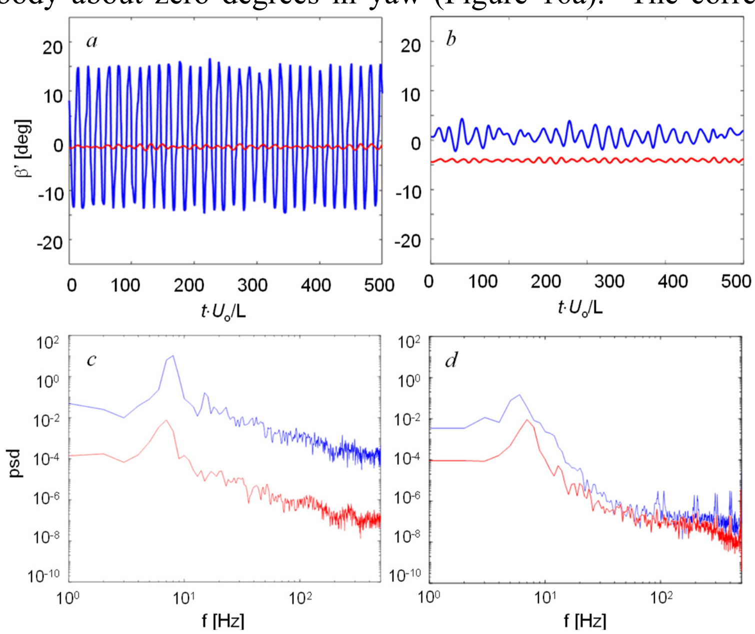

Figure 16. *Yaw traces (a,b) and power spectra (c,d) of the base (blue) and controlled (red) cases at α=53°, θ=90°, ϕ= 315° (a,c) and at α=60°, θ=90°, ϕ=240°(b,d).*

responds to the changing aerodynamic loads and it is not necessarily steady with time either. One such example is shown in Figure 16b, where some moderate body deflections are recorded in the uncontrolled state. It is interesting that application of the flow control to this state further stabilizes even these moderate deflections, but it also introduces a bias in the model yaw orientation, as the controlled model points to close to $\beta' = -4°$ orientation. Spectral analysis for these two states is shown in Figure 16d, where the base flow indicates oscillations at about 6 Hz and in general much lower energy levels across all frequencies compared to the uncontrolled unstable case (Figure 16c). In addition, as already stated in discussion of Figure 5, additional characteristic frequencies about 100 Hz (and their harmonics) could be tied to the natural shedding vortices off the body. Once the body is stabilized, the low frequency content of the uncontrolled flow becomes attenuated, while the dominant frequency, interestingly, shifts slightly higher to about 7 Hz. Another noteworthy observation is that the spectra for both of the controlled states (spectra in red) are nearly identical, in spite of the uncontrolled two states being vastly different.

V. Conclusions

The present experimental investigations build the on earlier findings of Lee et al. (2021), who demonstrated modification of the aerodynamic loads on slender axisymmetric bodies at high incidence by exploiting the receptivity of the forebody vortices to fluidic actuation at the forebody juncture. These investigations use a wire-mounted wind tunnel models that can respond to the changing aerodynamic loads. In some instances, the coupling between the body and its near wake can trigger dynamic unstable responses.

The present work focuses on flow interactions over a slender axisymmetric cylinder model ($L/D = 11$) with a tangent ogive forebody ($l/D = 2$) with emphasis on control of the unstable coupling between the cylinder and the forebody vortex pair within a range of high inclination angles ($45° < \alpha < 60°$). Actuation is effected by an azimuthally-rotatable synthetic jet that is integrated into the juncture between the forebody and the cylinder and is intended to affect the interaction of the forebody vortices with the cylinder's leeward-side near-wake, and consequently the aerodynamic loads on the body. The jet's azimuthal orifice spans 45º of the circumference (measuring 0.6×15.7 mm) and it is operating at 2.3 kHz.

As shown by earlier investigators, at high inclination angles the rollup of the counter-rotating forebody vortex pair becomes asymmetric and their interactions with the cylinder induce a nominally-stable side force whose sense depends on and varies with the azimuthal orientation of the forebody. The present investigations show that the unstable side force generally occurs when the azimuthal orientation of the forebody is set about where the side force switches its direction. While a nominally stable body is associated with a stable forebody vortex pair, during unsteady nearly-harmonic yaw oscillations, the forebody vortices undergo bimodal switching about the forebody. The instability is investigated when the cylinder undergoes a pitch up/down motion through a range in which the incidence results in instability, followed by detailed investigations at several fixed angles of attack.

During the pitch up/down maneuver in the absence of control there is a clear hysteresis in the onset and termination of the cylinder's instability in which the unstable domain is shifted to lower pitch angles during the pitch down maneuver, compared to its onset during pitch up motion. It is shown that the actuation completely bypasses the instability in either direction. Stereo PIV measurements in the wake downstream of the cylinders back end show that when the cylinder is stabilized, the wake vortices become stable as well. In addition, when the actuation is applied following the onset of the instability during pitch, it still leads to stabilization of the model and the wake vortices within 8-10 oscillation cycles, and following the removal of the actuation the unstable oscillations resume within 4-5 cycles. Similarly, when the cylinder is set at a fixed nominal incidence at which it is unstable, the instability is intermittently suppressed with repeated intermittent applications of the actuation. These results suggest that the direct control of the interactions of the forebody vortices with the near wake of the cylinder can be adopted for control of such instabilities in free flight.

Acknowledgment

This work was supported by the Army Research Office (monitored by Dr. M. Munson).

References

Almosnino, D. and Rom, J., "Lateral Forces on a Slender Body and Their Alleviation at High Incidences", J. Spacecraft and Rockets, **5**, 1981.

Deng, X., Wang, G., Chen, X., Wang, Y., Liu, P. and Xi, Z., “A Physical Model of Asymmetric Vortices Flow Structure in Regular State over Slender Body at High Angle of Attack,” *Sci. China E: Technological Sciences*, **46**, 2003.

Fagley, C., Farnsworth, J., Seidel, J. and McLaughlin, T., “Experimental Study of Open Loop Plasma Actuation on a von Kármán Ogive,” AIAA Paper 2012-0905, January 2012.

Kalyankar, H., Taubert, L. and Wygnanski, I., “Re-orienting the Turbulent Flow over an Inclined Cylinder of Finite Aspect Ratio,” AIAA Paper 2018-4026, June 2018.

Lambert, T.J., Vukasinovic, B., and Glezer, A., “A Six Degrees of Freedom Dynamic Wire-Driven Traverse,” *Aerospace,* **3**:11, 2016.

Lambert, T.J., Vukasinovic, B., and Glezer, A., “Aerodynamic Flow Control of Wake Dynamics Coupled to a Moving Bluff Body,” *AIAA Paper* 2016-4081.

Lambert, T., Vukasinovic, B., & Glezer, A., “A freely yawing axisymmetric bluff body controlled by near-wake flow coupling”. Journal of Fluid Mechanics, **863**, pp 1123-1156, 2019.

Lamont, P. and Kennaugh, A., “Multiple solutions for aircraft sideslip behavior at high angles of attack,” AIAA Paper 89-0645, Jan 1989.

Lee, E., Huang, Y., Vukasinovic, B., and Glezer, A., “Controlled Aerodynamic Loads on a Slender Axisymmetric Body at High Incidence,” AIAA 2021-1943. AIAA Scitech 2021 Forum, Jan 2021.

Leu, T.-S., Chang, J.-R. and Lu, P.-J., “Experimental Investigation of Side Force Control on Cone-Cylinder Slender Bodies with Flexible Micro Balloon Actuators,” *Exp. Ther. Fl. Sci.*, **29**, 2005.

Ma, B.-F. and Liu, T.-X., “Low-Frequency Vortex Oscillation around Slender Bodies at High Angles-of-Attack,” *Phys. Fluids,* **26**, 2014.

Mahadevan, S., Rodriguez,J. and Kumar, K., “Effect of Controlled Imperfections on the Vortex Asymmetry of a Conical Body,” *AIAA J.* **56**, pp. 3460-3477, 2018.

Nelson, R. and Fleeman, E., “High Angle-of-Attack Aerodynamics on a Slender Body with a Jet Plume,” *J. Spacecraft,* **12**, 1975.

Porter, C., Fagley, C., Farnsworth, J., Seidel, J. and McLaughlin, T., “Closed-Loop Flow Control of a Forebody at a High Incidence Angle,” *AIAA J.*, **52**, 2014.

Rao, D., Moskovitz, C. and Murri, D., “Forebody Vortex Management for Yaw Control at High Angles of Attack,” *J. Aircraft*, **24**, No. 4, pp. 248-254, April 1987.

Sato, A., Nishida, H. and Nonaka, S., “Preliminary Study on Aerodynamic Control of High-Angle-of-Attack Slender Body using Blowing from Penetrating Flow Channels,” *Int. J. Aero Eng*, 1602043, 2016.

Schnepf, C. and Schülein, E., “Numerical Study on the Impact of a Maneuver on the Phantom-Yaw-Effect in Transonic Flow,” AIAA Paper 2018-4124, June 2018.

Seidel, Jürgen, and Thomas Mclaughlin, “Feedback Flow Control: A Heuristic Approach.” *AIAA Journal*, arc.aiaa.org/doi/10.2514/1. J056884. 29 June 2018.

Skow, A., Moore, W. and Lorincz, D., “Control of Forebody Vortex Orientation to Enhance Departure Recovery of Fighter Aircraft,” *J. Aircraft*, **19**, 1982.

Stucke, R., “High Angle-of-Attack Yaw Control using Strakes on Blunt-Nose Bodies,” Ph.D. Dissertation, Univ. of Toledo, December 2006.

Thomson, K.D. and Morrison, D.F. “The Spacing, Position and Strength of Vortices in the Wake of Slender Cylindrical Bodies at Large Incidence,” *J. Fluid Mech*, **60**, 1971.

Ward, K. and Katz, J., “Development of Flow Structures in the Lee of an Inclined Body of Revolution”, *J. Aircraft*, **26**, 1989.

Williams, D., El-Khabiry, S. and Papazian, H., "Control of Asymmetric Vortices Around a Cone-Cylinder Geometry with Unsteady Base Bleed," AIAA Paper 89-1004, March 1989.

Williams, D. and Papazian, H., "Forebody Vortex Control with the Unsteady Bleed Technique," *AIAA J.*, **29**, 1991.

Wu, G., Wang, T. and Tian, S., “Investigation of Vortex Patterns on Slender Bodies at High Angles of Attack,” *J. Aircraft,* **23**, 1986.

Yanta, W. and Wardlaw, A., “Laser Doppler Velocimeter Measurements of Leeward Flowfields on Slender Bodies at Large Angle-of-Attack,” AIAA Paper 77-0668, June 1977.

Yanta, W. and Wardlaw, A., “Flowfield about and Forces on Slender Bodies at High Angles of Attack,” *AIAA J.*, **19**, 1981.

Yanta, W. and Wardlaw, A., “The Secondary Separation Region on a Body at High Angles of Attack,” AIAA Paper 82-0343, January 1982.

Zilliac, G., Degani, D. and Tobak, M., “Asymmetric Vortices on a Slender Body of Revolution,” *AIAA J.*, **29**, May 1991.